Atmos. Meas. Tech. Discuss., 7, 4407–4438, 2014
www.atmos-meas-tech-discuss.net/7/4407/2014/
doi:10.5194/amtd-7-4407-2014

Atmospheric Measurement Techniques Discussions

An inverse modelling approach for frequency response correction of capacitive humidity sensors in ABL research with small unmanned aircraft

N. Wildmann, F. Kaufmann, and J. Bange

Center for Applied Geoscience, Eberhard-Karls-Universität Tübingen, Tübingen, Germany

Received: 29 January 2014 – Accepted: 9 April 2014 – Published: 5 May 2014

Correspondence to: N. Wildmann (norman.wildmann@uni-tuebingen.de)

Published by Copernicus Publications on behalf of the European Geosciences Union.

Abstract

The measurement of water-vapour concentration in the atmosphere is an ongoing challenge in environmental research. Satisfactory solutions are present for ground-based meteorological stations and measurements of mean values. However, advanced research of thermodynamic processes also aloft, above the surface layer and especially in the atmospheric boundary layer (ABL), requires the resolution of small-scale turbulence. Sophisticated optical instruments are used in airborne meteorology with manned aircraft to achieve the necessary fast response measurements in the order of 1 Hz (e.g. LiCor 7500). Since these instruments are too large and heavy for the application on the promising platforms of small remotely piloted aircraft (RPA), a method is presented in this study, that enhances small capacitive humidity sensors to be able to resolve turbulent eddies in the order of 10 m. For this purpose a physical and dynamical model of such a sensor is described and inverted in order to restore original water vapour fluctuations from sensor measurements. Examples of flight measurements show how the method can be used to correct vertical profiles and resolve turbulence spectra up to about 3 Hz.

1 Introduction

1.1 Water vapour in atmospheric research

The atmospheric boundary layer (ABL) is in direct contact to the earth surface and therefore subject to water exchange with the soil, rivers, lakes and oceans. Although it is decoupled by a temperature inversion from the free atmosphere (upper troposphere), entrainment processes lead to an exchange of water vapour through the inversion (Stull, 1988). This exchange of water, enforced by turbulent transport in the ABL, leads to a high temporal, horizontal and vertical variability of water vapour. The water vapour concentration is not only important for cloud formation, rainfall and fog, it plays an

AMTD
7, 4407–4438, 2014

important role in the energy balance of the earth surface and for further thermodynamic processes in the atmosphere. Recent Large Eddy Simulations (LES) showed how the structure parameter of humidity is much less understood than the structure parameter of temperature. ABL structure is typically described by the means of similarity theories and parametrisations (Garratt, 1992) to be able to compare results in different regimes and different experiments. While for example the Monin–Obukhov similarity theory is found to be valid in all regimes for temperature, the same theory does not apply to humidity, especially if entrainment into the mixed layer is present (Maronga, 2014). A more distinct description of entrainment processes is needed, which will need precise measurements of water vapour fluxes to validate the models. Recently, first measurements of entrainment processes with small RPA were reported (Martin et al., 2014), but only temperature and wind could be analyzed, due to a lack of fast response humidity measurements. Essential for the measurement of turbulent fluctuations is a high sampling rate with short time responses throughout the measurement chain, high measurement resolution and accuracy, of course.

1.2 Water vapour measurement in airborne systems

In-situ measurement of atmospheric processes above the surface layer requires airborne sensor carriers in the form of fixed wing aircraft, helicopters, balloons or other. Examples for research aircraft for boundary-layer research are the Dornier 128 (Bange et al., 2002; Corsmeier et al., 2001), the DLR HALO (Kiemle et al., 2011), or the MetAir Dimona (Neininger et al., 2001). A slightly different type of airborne system that was used for ABL research is the helicopter probe Helipod (Bange and Roth, 1999). All of them are carrying at least one instrument to investigate water vapour and its fluxes in the ABL. An overview of the state of the art of instrumentation for airborne measurements is given in Bange et al. (2013) and a short summary is presented in Sect. 2.1 in this article. It has to be noted that manned research aircraft are subject to high operating cost and thus are only used in short, dedicated field experiments. Within the last decade, technical progress made it possible to use small remotely piloted aircraft

AMTD
7, 4407–4438, 2014

(RPA), equipped with autopilots and waypoint navigation, for research purposes in many fields (Martin et al., 2011, 2014; Martin and Bange, 2014; van den Kroonenberg et al., 2011, 2008; Spieß et al., 2007; Jonassen, 2008; Chao et al., 2008; Jensen and Chen, 2013). Their flexibility and low operating cost enables researchers to come up with new, innovative ideas to probe the atmosphere in a way that was not possible before. Along with these possibilities go challenges for instrumentation to become even smaller and more lightweight to be carried on these aircraft and still compete with the quality of ground based sensors. The smallest of these unmanned aerial vehicles (UAVs) as they are also called, weigh up to 6 kg and carry capacitive humidity sensors of different kinds (Reuder et al., 2009; Martin et al., 2011). In larger RPA, up to 50 kg, more sophisticated sensors like Krypton hygrometers can be carried (Thomas et al., 2012), that are too large for the smaller RPA. Small RPA (e.g. up to 5 kg) have several advantages: it is comparatively easy to achieve a flight permission for them in Central Europe. They do not require special ground facilities like a catapult or a runway. And they are low-cost. Furthermore, small RPA do not disturb the turbulent flow they have to measure, which increases accuracy, if at the same time the sensors allow a fast response measurement of the variable of interest. This shows that an improved response time for capacitive humidity sensors can be of great benefit for atmospheric research, and especially for turbulence measurements. At the University of Tübingen, the RPA MASC (Multi-purpose Airborne Sensor Carrier) is operated which is equipped with fast temperature sensors (Wildmann et al., 2013), a flow probe (Wildmann et al., 2014) and a capacitive humidity sensor. All flight measurements that are presented in this article were carried out with the MASC RPA.

1.3 Control theory and signal restoration

In this study, methods of control theory will be applied to achieve better results in the measurement of humidity with capacitive sensors. In control theory, mathematical models are derived from physical systems and put into standard forms to describe the dynamics of the system and eventually design controllers to influence the

AMTD
7, 4407–4438, 2014

behaviour. Instead of designing controllers for the system, the mathematical description of the dynamic behaviour of the system can also be used to restore the original signal from a measurement, if the dynamics of the sensor are well described. Similar work has been done in the field of airspeed measurement with flow probes (Rediniotis and Pathak, 1999) to correct for time delays in the pneumatic setup of these sensors. Another example are thermocouples in combustion engines where fast response of the sensors in harsh conditions is desired (Tagawa et al., 2005). It is shown in this report, how similar techniques can be applied for capacitive humidity sensors in ABL research. Compared to simple time delay corrections that were reported to be applied for capacitive humidity sensors in radiosondes (Leiterer et al., 2005), the approach to use control theory methods makes it possible to also model more complicated dynamics, which can be found for this type of sensors.

2 Water vapour measurement

2.1 State of the art

A variety of sensors is used to measure water-vapour concentration in the atmosphere. While psychrometers are used for mean measurement of relative humidity in most weather stations, the most widely used instrument for ground based flux measurements is the LI-7500A gas analyzer by the company Li-Cor®. In airborne measurements, a wide variety of customized instruments is being used, including e.g. Lyman-α absorption hygrometers (e.g. Bange et al., 2002), tunable diode laser absorption spectroscopy hygrometers (TDLAS, e.g. Zondlo et al., 2010; Paige, 2005), infrared absorption hygrometers (e.g. LI-7500A), chilled mirror dew point instruments (DPM, Neininger et al., 2001), krypton hygrometers (Thomas et al., 2012) or polymer based thin film capacitive absorption hygrometers (see Spieß et al., 2007; Reuder et al., 2009). The most recent and comprehensive study about hygrometers for airborne meteorology is probably the Aquavit experiment described in Fahey et al. (2009), that was carried out

AMTD
7, 4407–4438, 2014

at the facilities of the University of Karlsruhe. A total number of 25 instruments were compared in a climate chamber under laboratory conditions, including several TDLASs and Ly-α instruments, as well as a DPM. The results of this experiment show that even under laboratory conditions and with instruments that have been extensively used in field experiments, uncertainties of ±10 % are common and proper calibration is crucial, especially for the optical instruments. Additional sensor types that have not previously been mentioned and are found in ground-based meteorology are psychrometers, and resistive or inductive hygrometers.

2.2 Capacitive humidity sensors

Results like the ones from the Aquavit experiment show how even on large research aircraft with plenty of space and payload capibilities, the measurement of water-vapour concentration is subject to large errors and intense research. In any case, none of the instruments that are used on manned aircraft and therefore none of the instruments that were tested in the Aquavit experiment can easily be carried with small RPA, where compact size and light weight are essential. A trade-off has to be made regarding accuracy, response time and long-term stability of the sensors. Reflecting on Sect. 2.1, the sensor type which can be realized easiest for small RPA is the capacitive humidity sensor. The size of these elements is typically less than 1 cm^2 and in non-severe conditions, accuracy and stability of the elements is adequate.

Capacitive humidity sensors are in most cases based on thin film polymers (Tetelin and Pellet, 2006; Sen and Darabi, 2008; Shibata et al., 1996). The materials adsorb water at the sensor surface from where it diffuses into the material and changes the relative permittivity and therefore the capacitance of the sensor (see Sect. 2.3). With decreasing thickness of the polymer, the time constant also decreases. One of the fastest of this kind on the market is the P14 Rapid by Innovative Sensor Technology (IST) AG, which has a time response of < 1.5 s falling edge, according to the specification (Fig. 1 and Table 1). These sensors can be subject to hysteresis, as adsorption and desorption are not necessarily taking place with the same rate. They also might

AMTD
7, 4407–4438, 2014

show a certain temperature sensitivity. A quantification of these effects needs to be done for each sensor type, since the effects can differ a lot depending on the dielectrical material and the design of the element. Since the P14 Rapid sensor was found to be the most reliable and at the same time fastest sensor available, all experiments and assumptions were made using this particular sensor. The polymer type is a company secret, thus parts of the model derived in Sect. 2.3 rely on calibration and tests. The polymer thickness of 1 µm was inquired from IST. In the setup that was used for this study, the sensor is connected to the PCAP01 capacitance converter chip on a custom made printed circuit board (PCB, see Fig. 2). The converter measures the charge and discharge time of the capacitor in comparison to a known reference capacitance and provides the ratio of the two on a digital output. The digital signal is then processed by the in-house development AMOC (Airborne Meteorological Onboard Computer) where it is stored with 100 Hz onto an SD card. At the same time, the sensor signal can be monitored in real-time on a remote computer.

2.3 Physical model

In this chapter, the physical model of the sensor will be described. Since the dynamical model that will be presented in Sect. 3 describes the dynamics of the water concentration in the polymer for changes in environmental water-vapour pressure, it is necessary to find the relationship between measured capacitance of the sensor and water concentration in the polymer.

In a parallel-plate capacitor the charge per voltage is defined as the capacitance. It can also be expressed as a function of the area A of the parallel plate, the distance d between the plates, the relative permittivity ε_r of the material between the plates and the vacuum permittivity ε_0:

$$C = \frac{Q}{U} = \varepsilon_0 \varepsilon_r \frac{A}{d} = (\varepsilon_r - 1)\varepsilon_0 \frac{A}{d} + \varepsilon_0 \frac{A}{d}. \quad (1)$$

AMTD
7, 4407–4438, 2014

For the following studies, it helps to decompose the capacity of the humidity sensor into partial capacities (Eq. 2), in particular the capacitance of vacuum between the plates C_0, the capacitance of the polymer alone C_{Poly} and the capacitance of absorbed water in the polymer $C_{\mathrm{H_2O}}$. C_{Poly} and C_0 are constant and provide an offset capacitance for zero water concentration, while $C_{\mathrm{H_2O}}$ is accounting for the sensitivity of the capacitance to changes of water concentration in the polymer.

$$
\begin{aligned}
C &= \varepsilon_0 \varepsilon_{\mathrm{r}} \frac{A}{d} \\
C &= \varepsilon_0 \left(\varepsilon_{\mathrm{r}}^{\mathrm{H_2O}} + \varepsilon_{\mathrm{r}}^{\mathrm{Poly}} \right) \frac{A}{d} \\
C &= \underbrace{\varepsilon_0 \varepsilon_{\mathrm{r}}^{\mathrm{Poly}} \frac{A}{d}}_{:=C_{\mathrm{Poly}}} + \underbrace{\left(\varepsilon_{\mathrm{r}}^{\mathrm{H_2O}} - 1 \right) \varepsilon_0 \frac{A}{d}}_{:=C_{\mathrm{H_2O}}} + \underbrace{\varepsilon_0 \frac{A}{d}}_{:=C_0}.
\end{aligned}
\tag{2}
$$

The Debye-equation for molar polarisation P_{m} connects the microscopic characteristics electrical dipole moment α and polarisability μ to the relative permittivity ε_{r} of a matter (Debye, 1929).

$$
P_{\mathrm{m}} = \frac{\varepsilon_{\mathrm{r}}^{\mathrm{H_2O}} - 1}{\varepsilon_{\mathrm{r}}^{\mathrm{H_2O}} + 2} = \frac{Z}{3\varepsilon_0} \cdot \left(\alpha + \frac{\mu^2}{k_{\mathrm{B}} T} \right). \tag{3}
$$

with particle density $Z = \frac{\varrho}{M} N_{\mathrm{A}}$, and ϱ the density, M the moleculare mass, N_{A} the Avogadro constant, k_{B} the Boltzmann constant and T the temperature. $\varepsilon_{\mathrm{r}}^{\mathrm{H_2O}}$ can be derived from Eq. (2) to yield:

$$
\varepsilon_{\mathrm{r}}^{\mathrm{H_2O}} = \frac{(C - C_{\mathrm{Poly}})}{C_0}. \tag{4}
$$

AMTD
7, 4407–4438, 2014

The particle density Z can also be expressed as the integral of water concentration c in the volume:

$$Z(t) = \frac{\int_z \int_y \int_x c(x,y,z,t)\,\mathrm{d}x\,\mathrm{d}y\,\mathrm{d}z \cdot N_\mathrm{A}}{V}. \tag{5}$$

For spatially constant concentration ($\nabla c = 0$):

$$Z = \frac{c \cdot V \cdot N_\mathrm{A}}{V} = c \cdot N_\mathrm{A}. \tag{6}$$

With the help of Eqs. (2), (3) and (6), water concentration can be found as a function of capacitance and temperature:

$$c = \frac{\frac{(C - C_\mathrm{Poly})}{C_0} - 1}{\frac{(C - C_\mathrm{Poly})}{C_0} + 2} \cdot \frac{3\varepsilon_0}{\alpha + \frac{\mu^2}{k_\mathrm{B} T}} \cdot \frac{1}{N_\mathrm{A}} \tag{7}$$

While C is the actually measured capacitance, and C_0 is defined as $\varepsilon_0 \frac{A}{d}$, C_poly is unknown before calibration. It is estimated by extrapolation of the calibration regression to zero relative humidity. The calibration procedure is described in Sect. 2.4.

2.4 Calibration

Calibration is used to connect the water concentration on the sensor polymer surface to relative humidity in the environment. Diffusion into the polymer will lead to a balance of water concentration throughout the whole polymer after a finite time. The dynamics of this process are modelled in Sect. 3. For the calibration, a constant humidity is held for at least 30 min to assure equilibrium of the water concentration. Most polymer-based capacitive humidity sensors are optimized in the choice of the polymer to show a linear relationship between relative humidity and capacitance. This also applies for

AMTD
7, 4407–4438, 2014

the sensor under investigation. Figure 3 shows the result of three calibrations at three different temperatures. In each case, temperature is kept constant and relative humidity is stepwise increased from 15 % to 85 % in a climate chamber. A dew point mirror in conjunction with a PT100 temperature sensor inside the calibration chamber is used as reference instrument to control relative humidity and temperature. It arises that while sensor physics depend on both, temperature and water vapour partial pressure, the P14 Rapid was designed that the overall behaviour follows a linear behaviour with relative humidity within the calibrated temperature range.

3 Dynamic signal restoration

3.1 Dynamic model

A dynamic model describes the behaviour of a system over time. This behaviour is typically described mathematically by a set of differential equations. In the case of a capacitive humidity sensor, the dynamics are mainly influenced by the diffusion of water vapour from the sensor surface into the polymer. The diffusion flux J is described by the Fick's law, which for the one dimensional case can be described by Eq. (8). It is assumed that a one dimensional model with a spatially constant diffusion coefficient D describes the behaviour of the sensor well enough.

$$J = -D \cdot \frac{\partial c}{\partial x}, \tag{8}$$

Combined with the continuity equation of mass conservation (Eq. 9), the second Fick's law can be derived (Eq. 10).

$$\frac{\partial c}{\partial t} = -\frac{\partial J}{\partial x} \tag{9}$$

$$\frac{\partial c}{\partial t} = \frac{\partial}{\partial x}\left(D\frac{\partial c}{\partial x}\right) \tag{10}$$

AMTD
7, 4407–4438, 2014

Since this relation yields into a differential equation of second order, a simplification is needed to find a manageable solution. A common solution to these kind of problems is a numerical approach like the finite volume method (LeVeque, 2002). According to this method, the mass conservation Eq. (9) is integrated over a finite volume element V_i.

$$\int_{V_n} \frac{\partial c}{\partial t} \mathrm{d}V = -\int_{V_n} \frac{\partial J}{\partial x} \mathrm{d}V \tag{11}$$

The divergence theorem (or: the combination of the continuity equation with the Gauss theorem) allows to write the right hand side of the equation as a surface integral. The left hand side can be solved to be the product of spatial averaged concentration change in a volume element and its volume.

$$\frac{\partial \overline{c_n}}{\partial t} V_n = -\oint_S J \, \mathrm{d}S. \tag{12}$$

In the following, concentrations with an index always represent spatial averages over a finite volume element V_n and the overbar notation will be omitted.

The surface integral for the simple case of a one dimensional model equals to the sum of diffusion from the layer above $(n-1)$ and the layer below $(n+1)$ for each layer n and therefore yields:

$$\frac{\partial c_n}{\partial t} = \frac{-D \cdot \frac{c_n - c_{n-1}}{\Delta x} \cdot A_{n,n-1}}{V_n} + \frac{-D \cdot \frac{c_n - c_{n+1}}{\Delta x} \cdot A_{n,n+1}}{V_n}, \tag{13}$$

where $A_{n,n-1}$ and $A_{n,n+1}$ are the top and bottom surface area of the polymer layers respectively. A matrix representation of the simplified diffusion model with $Y = \frac{D \cdot A}{\Delta x \cdot V_n}$ is

AMTD
7, 4407–4438, 2014

given in Eq. (14).

$$\begin{pmatrix} \frac{\partial c_1}{\partial t} \\ \frac{\partial c_2}{\partial t} \\ \frac{\partial c_3}{\partial t} \\ \frac{\partial c_4}{\partial t} \\ \vdots \\ \vdots \\ \frac{\partial c_{N-1}}{\partial t} \\ \frac{\partial c_N}{\partial t} \end{pmatrix} = \begin{pmatrix} -2Y & Y & 0 & 0 & 0 & 0 & \cdots & 0 \\ Y & -2Y & Y & 0 & 0 & 0 & \cdots & 0 \\ 0 & Y & -2Y & Y & 0 & 0 & \cdots & 0 \\ 0 & 0 & Y & -2Y & Y & 0 & \cdots & 0 \\ \vdots & & & & \ddots & & & \vdots \\ \vdots & & & & & \ddots & & \vdots \\ 0 & 0 & 0 & 0 & \cdots & Y & -2Y & -Y \\ 0 & 0 & 0 & 0 & \cdots & 0 & Y & -Y \end{pmatrix} \cdot \begin{pmatrix} c_1 \\ c_2 \\ c_3 \\ c_4 \\ \vdots \\ \vdots \\ c_{N-1} \\ c_N \end{pmatrix} + \begin{pmatrix} Y \\ 0 \\ 0 \\ 0 \\ \vdots \\ \vdots \\ 0 \\ 0 \end{pmatrix} \cdot c_s \tag{14}$$

$$c_m = (1\ 1\ 1\ \cdots\ 1) \begin{pmatrix} \frac{c_1}{N} \\ \frac{c_2}{N} \\ \frac{c_3}{N} \\ \vdots \\ \frac{c_N}{N} \end{pmatrix}$$

Boundary conditions exist for the layer at the surface of the sensor and the bottom most layer. At the surface layer the concentration that is adsorped from ambient water vapour diffuses into the layer. At the bottom, no diffusion is possible from below. Figure 4 shows a sketch of the one dimensional model of finite volumes in the sensor polymer.

Equation (14), translated to vector notation, is conform with the standard layout of a single-input-single-output (SISO) state-space model, as it is used in control theory

AMTD
7, 4407–4438, 2014

(Lutz and Wendt, 2007):

$$\frac{\partial}{\partial t}\boldsymbol{c} = \mathbf{Y}\boldsymbol{c} + (Y\ 0\ 0\ \cdots\ 0)^T c_\mathrm{s}$$
$$c_\mathrm{m} = \left(\frac{1}{N}\ \frac{1}{N}\ \frac{1}{N}\ \cdots\ \frac{1}{N}\right)\boldsymbol{c} \tag{15}$$

The vector $\boldsymbol{c}$ of water concentrations in each layer of the model is the state vector. The diffusion matrix $\mathbf{Y}$ is the system (or state) matrix, which describes how the current concentrations $\boldsymbol{c}$ in each layer affect the change in concentrations $\frac{\partial}{\partial t}\mathbf{c}$. The input (or control) vector $(Y\ 0\ 0\ \cdots\ 0)^T$ determines how the system input affects the states $\boldsymbol{c}$. It is modelled to describe the diffusion of water vapour into the top most layer of the sensor. The single input variable of the whole system is the surface concentration c_s and the single output variable is the total water concentration in the polymer c_m, that is presented to be a function of the measured capacitance in Eq. (7). The so-called output vector $\left(\frac{1}{N}\ \frac{1}{N}\ \frac{1}{N}\ \cdots\ \frac{1}{N}\right)$ maps the states $\mathbf{c}$ to the output variable c_m, which in the case of the sensor model is a simple averaging of the concentrations in all layers.

3.1.1 Model validation

To show that this model does fit with reality, step response experiments with rising and falling edge steps of humidity were performed. The results in Fig. 5 show that the model fits well with reality, if the correct diffusion coefficient is applied. Of course, it has to be noted that the diffusion coefficient, since it is the one unknown parameter in the model, also serves as a correction factor for other model inaccuracies and therefore is most likely not the true physical diffusion coefficient. Remaining deviations between model and measurement can also result from a non-perfect step input. For the experiment, a humidity sensor was placed in a very small chamber ($< 2\,\mathrm{cm}^3$) at ambient humidity. At time 0 the chamber is flooded with air of well defined humidity from the dew point generator, which is also used for calibration. The sensor is presumed to be flooded in

AMTD
7, 4407–4438, 2014

less than 100 ms considering the outlet flow of the generator and the size of the chamber. Comparing the rising and falling edge steps, it becomes evident that no difference in time response can be observed for both cases, and the model works with the same diffusion coefficient without hysteresis. This implies that diffusion is the dominant factor in comparison to adsorption and desorption regarding the dynamics of the sensor, and the model is suitable to describe the dynamic behaviour of the sensor.

To investigate the sensitivity of the diffusion coefficient to ambient temperature, tests were done at two different temperatures (5 °C and 20 °C). The result in Fig. 6 shows that, like expected, the diffusion coefficient is lower for decreased ambient temperature. This means that it is not possible to apply a universal diffusion coefficient for one sensor, but the diffusion coefficient needs to be adapted to the given ambient temperature.

3.2 Inverse model for signal restoration

Having found a model that reasonably describes the dynamic behaviour of the sensor, it is now possible to use this model to restore the original signal of relative humidity in the atmosphere from measured data. For this purpose it is necessary to invert the model, which is equivalent to solving the system equations for the original water vapour concentration c_s.

Since the state-space model cannot easily be inverted, the first step is to transform Eq. (15) to a transfer function in the Laplace domain. This can be done as presented in Eq. (16) according to Lutz and Wendt (2007).

$$c_m(s) = \underbrace{\left(\frac{1}{N}\ \frac{1}{N}\ \cdots\ \frac{1}{N}\right)(s\mathbf{E}-\mathbf{Y})^{-1}(Y\ 0\ \cdots\ 0)^T}_{G(s)} \cdot c_s(s) \qquad (16)$$

$$c_m(s) = G(s) \cdot c_s(s)$$

E is a unity matrix of same dimensions as the system matrix **Y**. The variable s is a result of the Laplace transformation. $G(s)$ is the transfer function in Laplace domain. The charm of transforming the system equation into the Laplace domain is that for linear

AMTD
7, 4407–4438, 2014

dynamic systems (LDSs) – like the sensor model in this study – simple mathematical operations can be applied in the Laplace domain, to solve complex tasks. A transfer function of a LDS can be expressed as a fraction with a numerator and a denominator polynomial of the parameter s. This fraction can simply be inverted to solve Eq. (16) for the original signal:

$$c_s(s) = G(s)^{-1} \cdot c_m(s) \tag{17}$$

A drawback of this method is that it only works well, if the measured signal and the applied model fit well. Noise that is not modelled will be amplified more with increasing order of the polynomial in the transfer function. On the other hand the model will be more accurate with a higher number of modelled layers in the polymer, which leads to a high polynomial order in the transfer function. A way to deal with this problem is oversampling and careful filtering of the measured signal, in order to achieve a good signal to noise ratio.

Figure 7 shows a block diagram of the signal restoration including input and output filters that were applied to achieve a restored signal that is not disturbed by amplified noise of the inverse modelling. For the input, a sharp low pass filter of 20th order at cutoff frequency 10 Hz is chosen to eliminate the white noise of the capacitance measurement, which dominates above this frequency. In the output filter a first order low pass is good enough to filter remaining noise after the signal restoration.

4 Results

4.1 Vertical profiles

For vertical profiles, slow dynamics of sensors lead to blurred measurements with either overestimated or underestimated water vapour concentration at each altitude, depending on the lapse rate. The effect shows clearly if RPA flights are used with consecutive ascends and descends. The sensor dynamics result in a hysteresis between ascend

AMTD
7, 4407–4438, 2014

and descend measurement of relative humidity. In the past it was common practice to either simply take the average between ascend and descend flights, which gives a good approximation for the true value, or apply some time delay correction of first order as described in Jonassen (2008) for RPA and in Leiterer et al. (2005) for radiosondes. The method described in Sect. 3 can be applied for this purpose as well. In Fig. 8 a vertical profile is shown with raw measurements and with restored signal for relative humidity. It clearly shows how a present offset between ascend and descend of the flight is eliminated in almost every detail, except for a few altitudes, where obviously local events of water vapour disturb the continuity of the profile, so to see between 150 and 200 m or at 350 m barometric altitude. The critical parameter to tune for the sensor model is the diffusion coefficient as described above. Within a minute or two that are needed for an ascend and a descend of a vertical profile with the RPA, in a not convective boundary layer, the mean relative humidity will not shift into one direction or the other, so that the parameter can be tuned to show a minimum offset between ascend and descend. Once the diffusion coefficient is found from a vertical profile it is found to be possible to use this parameter for the signal restoration of the complete flight with a duration of 30–60 min. It is however recommended to redo the vertical profile diffusion coefficient estimation for each flight, since contaminations and small damages invisible to the human eye were found to significantly change the sensor dynamics. Different sensors of the same batch can even show slightly different characteristics.

4.2 Spectral response

A MASC RPA at the University of Tübingen is equipped with fast sensors for temperature and wind measurement for turbulence measurement. One goal of this study is to make turbulence studies for water vapour possible with capacitive humidity sensors. To quantify the improvements that were achieved towards this goal, it is useful to investigate the spectral response of the sensor before and after the signal restoration. Figure 9 shows the power spectral density of the relative humidity signal over the frequency for both cases. The original signal is strongly affected by the slow sensor dynamics for

AMTD
7, 4407–4438, 2014

frequencies above 0.05 Hz. At about 3 Hz the signal vanishes in noise entirely (spectral power is almost constant for higher frequencies). The restored signal is almost perfectly following the expected $-5/3$ slope for locally isotropic turbulence in the inertial subrange according to Kolmogorov (1941), until about 3 Hz. For higher frequencies, noise is dominant and thus the limiting factor of the signal restoration.

Another method to show the distribution of turbulent energy on different scales is the structure function according to Kolmogorov (1941). Even more clearly than for the power spectral densities, deviations of the measured values from the theoretical slope for locally isotropic turbulence in the inertial subrange, which in the case of the double-logarithmically plotted structure function is 2/3, are a strong indication for sensor dynamics or other errors in the measurement. Figure 10 shows how close the structure function of the restored signal is to the theory until a time lag of about 0.3 s (corresponding to 3 Hz), especially compared to the original signal.

5 Conclusions

This report addressed the problem of water-vapour measurement for turbulence analysis with small remotely piloted aircraft (RPA). It was identified that capacitive humidity sensors are the currently only feasible solution for these measurements onboard an RPA of 5 kg as it is operated in Tübingen or smaller. A method is introduced to enhance the quality of such measurements with the help of control theory methods in post-processing. In order to apply these enhancements, a more detailed understanding of the sensor is needed, which is presented as a physical model describing the sensitivity of permittivity of a polymer to changes in water concentration in Sect. 2.3 and a dynamical model describing the diffusion of water from the sensor surface into the polymer in Sect. 3. On the base of this model, a method to restore the original signal from measurements is presented. It is shown in Sect. 4 how vertical profiles can be corrected using the presented method. It is proposed to use a minimization of error between ascend and descend of a vertical profile flight with an RPA to find the correct

AMTD
7, 4407–4438, 2014

diffusion coefficient for the given temperature and sensor. This is necessary, since the exact relation between diffusion coefficient and temperature could not be determined in a laboratory experiment and information about the polymer type is not available. The benefit of determining the diffusion coefficient empirically for each measurement flight is that this parameter is the only unknown in the model and therefore can also be used to correct for other inaccuracies in the model. A spectral analysis of flight legs in the atmospheric boundary layer with a diffusion coefficient determined from a vertical profile in the same flight showed promising results for turbulence analysis. It can be stated that the enhancement of the sensor makes it possible to resolve turbulent fluctuations up to 3 Hz. Compared to temperature and wind measurement on a MASC RPA (up to 20 Hz), this is still fairly low and will need to be improved in future work. The main constraints for the given setup is the signal to noise ratio and sensitivity of the capacitance measurement. Improvements on the measurement circuit with several sensors in parallel can possibly solve this problem. Measurements of turbulent fluctuations up to 10 Hz seem possible. The systematic approach of the signal restoration is open to further extensions of the sensor model e.g. physical descriptions of water adsorption on the sensor surface or temperature dependence of diffusion into the polymer.

Acknowledgements. We would like to thank Maximilian Ehrle and Markus Auer for their great job as safety pilot in the test flights. The measuring equipment would not have been ready to work without the help of Jens Dünnermann and Burkhard Wrenger from the University of Applied Sciences Ostwestfalen-Lippe.

We acknowledge support by Deutsche Forschungsgemeinschaft and Open Access Publishing Fund of Tuebingen University.

References

Bange, J. and Roth, R.: Helicopter-borne flux measurements in the nocturnal boundary layer over land – a case study, Bound.-Lay. Meteorol., 92, 295–325, 1999. 4409

AMTD
7, 4407–4438, 2014

Bange, J., Beyrich, F., and Engelbart, D. A. M.: Airborne measurements of turbulent fluxes during LITFASS-98: a case study about method and significance, Theor. Appl. Climatol., 73, 35–51, 2002. 4409, 4411

Bange, J., Esposito, M., and Lenschow, D. H.: Airborne Measurements for Environmental Research – Methods and Instruments, chap. 2: Measurement of Aircraft State, Thermodynamic and Dynamic Variables, 641 pp., Wiley, 2013. 4409

Chao, H., Baumann, M., Jensen, A., Chen, Y., Cao, Y., Ren, W., and McKee, M.: Band-reconfigurable multi-UAV-based cooperative remote sensing for real-time water management and distributed irrigation control, IFAC World Congress, Seoul, Korea, 2008. 4410

Corsmeier, U., Hankers, R., and Wieser, A.: Airborne turbulence measurements in the lower troposphere onboard the research aircraft Dornier 128-6, D-IBUF, Meteorol. Z., 4, 315–329, 2001. 4409

Debye, P.: Polare Molekeln, S. Hirzel, Leipzig, 1929. 4414

Fahey, D., Gao, R., and Möhler, O.: Summary of the AquaVIT Water Vapor Intercomparison: Static Experiments, Aquavit White Paper, available at: https://aquavit.icg.kfa-juelich.de/AquaVit/AquaVitWiki (last access: 29 April 2014), 2009. 4411

Garratt, J.: The Atmospheric Boundary Layer, University Press, Cambridge, 1992. 4409

Jensen, A. and Chen, Y.: Tracking tagged fish with swarming unmanned aerial vehicles using fractional order potential fields and Kalman filtering, in: 2013 International Conference on Unmanned Aircraft Systems (ICUAS), IEEE, 1144–1149, 2013. 4410

Jonassen, M. O.: The Small Unmanned Meteorological Observer (SUMO), Master's thesis, University of Bergen, Geophysical Institute, 2008. 4410, 4422

Kiemle, C., Wirth, M., Fix, A., Rahm, S., Corsmeier, U., and Di Girolamo, P.: Latent heat flux measurements over complex terrain by airborne water vapour and wind lidars, Q. J. Roy. Meteor. Soc., 137, 190–203, doi:10.1002/qj.757, 2011. 4409

Kolmogorov, A.: The local structure of turbulence in incompressible viscous fluid for very large Reynolds Numbers, Dokl. Akad. Nauk SSSR, 30, 299–303, 1941, reprint: P. Roy. Soc. A, 434, 9–13, 1991. 4423

Leiterer, U., Dier, H., Nagel, D., Naebert, T., Althausen, D., Franke, K., Kats, A., and Wagner, F.: Correction method for RS80-A Humicap humidity profiles and their validation by lidar backscattering profiles in tropical cirrus clouds, J. Atmos. Ocean. Tech., 22, 18–29, 2005. 4411, 4422

AMTD
7, 4407–4438, 2014

LeVeque, R. J.: Finite Volume Methods for Hyperbolic Problems, Cambridge University Press, doi:10.1017/CBO9780511791253, 2002. 4417
Lutz, H. and Wendt, W.: Taschenbuch der Regelungstechnik: mit MATLAB und Simulink, Harri Deutsch, Frankfurt am Main, Germany, 2007. 4419, 4420
Maronga, B.: Monin–Obukhov similarity functions for the structure parameters of temperature and humidity in the unstable surface layer: results from high-resolution large-eddy simulations, J. Atmos. Sci., 71, 716–733, 2014. 4409
Martin, S., Bange, J., and Beyrich, F.: Meteorological profiling of the lower troposphere using the research UAV "M^2AV Carolo", Atmos. Meas. Tech., 4, 705–716, doi:10.5194/amt-4-705-2011, 2011. 4410
Martin, S. and Bange, J.: The Influence of Aircraft Speed Variations on Sensible Heat-Flux Measurements by Different Airborne Systems, Bound.-Lay. Meteorol., 150, 153–166, doi:10.1007/s10546-013-9853-7, 2014a. 4410
Martin, S., Beyrich, F., and Bange, J.: Observing Entrainment Processes Using a Small Unmanned Aerial Vehicle: A Feasibility Study, Bound.-Lay. Meteorol., 150, 449–467, doi:10.1007/s10546-013-9880-4, 2014b. 4409, 4410
Neininger, B., Fuchs, W., Baeumle, M., Volz-Thomas, A., Prévôt, A. S. H., and Dommen, J.: A small aircraft for more than just ozone: MetAir's "Dimona" after ten years of evolving development, in: 11th Symp. on Meteorological Observations and Instrumentation, Albuquerque, NM, Amer. Meteor. Soc., 123–128, 2001. 4409, 4411
Paige, M. E.: Compact and low-power diode laser hygrometer for weather balloons, J. Atmos. Ocean. Techn., 22, 1219–1224, doi:10.1175/jtech1770.1, 2005. 4411
Rediniotis, O. and Pathak, M.: Simple technique for frequency-response enhancement of miniature pressure probes, AIAA J., 37, 897–899, 1999. 4411
Reuder, J., Brisset, P., Jonassen, M., Müller, M., and Mayer, S.: The Small Unmanned Meteorological Observer SUMO: a new tool for atmospheric boundary layer research, Meteorol. Z., 18, 141–147, 2009. 4410, 4411
Sen, A. and Darabi, J.: Modeling and optimization of a microscale capacitive humidity sensor for HVAC applications, IEEE Sens. J., 8, 333–340, 2008. 4412
Shibata, H., Ito, M., Asakursa, M., and Watanabe, K.: A digital hygrometer using a polyimide film relative humidity sensor, IEEE T. Instrum. Meas., 45, 564–569, 1996. 4412
Spieß, T., Bange, J., Buschmann, M., and Vörsmann, P.: First Application of the Meteorological Mini-UAV "M2AV", Meteorol. Z., 16, 159–169, 2007. 4410, 4411

AMTD
7, 4407–4438, 2014

Stull, R.: An Introduction to Boundary Layer Meteorology, Kluwer Acad., Dordrecht, 1988. 4408
Tagawa, M., Kato, K., and Ohta, Y.: Response compensation of fine-wire temperature sensors, Rev. Sci. Instrum., 76, 094904, doi:10.1175/JAS-D-13-0135.1, 2005. 4411
Tetelin, A. and Pellet, C.: Modeling and optimization of a fast response capacitive humidity sensor, IEEE Sens. J., 6, 714–720, 2006. 4412
Thomas, R. M., Lehmann, K., Nguyen, H., Jackson, D. L., Wolfe, D., and Ramanathan, V.: Measurement of turbulent water vapor fluxes using a lightweight unmanned aerial vehicle system, Atmos. Meas. Tech., 5, 243–257, doi:10.5194/amt-5-243-2012, 2012. 4410, 4411
van den Kroonenberg, A. C., Martin, T., Buschmann, M., Bange, J., and Vörsmann, P.: Measuring the wind vector using the autonomous mini aerial vehicle M^2AV, J. Atmos. Oceanic Technol., 25, 1969–1982, 2008. 4410
van den Kroonenberg, A., Martin, S., Beyrich, F., and Bange, J.: Spatially-averaged temperature structure parameter over a heterogeneous surface measured by an unmanned aerial vehicle, Bound.-Lay. Meteorol., 142, 55–77, 2011. 4410
Wildmann, N., Mauz, M., and Bange, J.: Two fast temperature sensors for probing of the atmospheric boundary layer using small remotely piloted aircraft (RPA), Atmos. Meas. Tech., 6, 2101–2113, doi:10.5194/amt-6-2101-2013, 2013. 4410
Wildmann, N., Ravi, S., and Bange, J.: Towards higher accuracy and better frequency response with standard multi-hole probes in turbulence measurement with remotely piloted aircraft (RPA), Atmos. Meas. Tech., 7, 1027–1041, doi:10.5194/amt-7-1027-2014, 2014. 4410
Zondlo, M. A., Paige, M. E., Massick, S. M., and Silver, J. A.: Vertical cavity laser hygrometer for the National Science Foundation Gulfstream-V aircraft, J. Geophys. Res., 115, D20309, doi:10.1029/2010JD014445, 2010. 4411

AMTD
7, 4407–4438, 2014

Table 1. Overview of P14 Rapid characteristics.

size	approx. 3 mm × 2 mm
active element area	6×10^{-6} m^2
thickness	1 µm
material	unknown polymer
specified response time	< 1.5 s

AMTD
7, 4407–4438, 2014

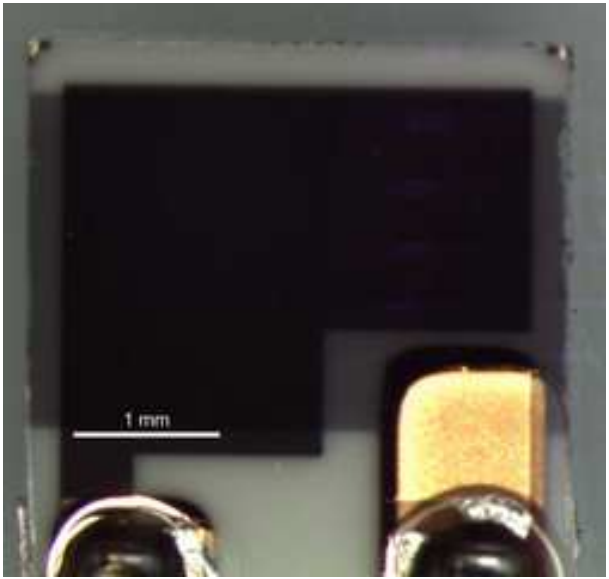

Fig. 1. Sensitive element of a capacitive humidity sensor. The black polygon is the polymer between two gold electrodes.

AMTD
7, 4407–4438, 2014

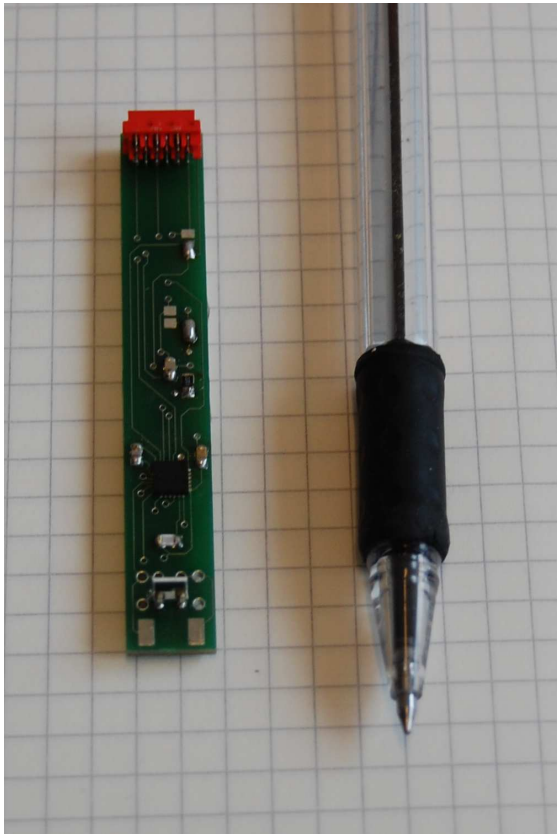

Fig. 2. Humidity sensor on printed circuit board with the capacitance measurement chip PCAP01.

AMTD
7, 4407–4438, 2014

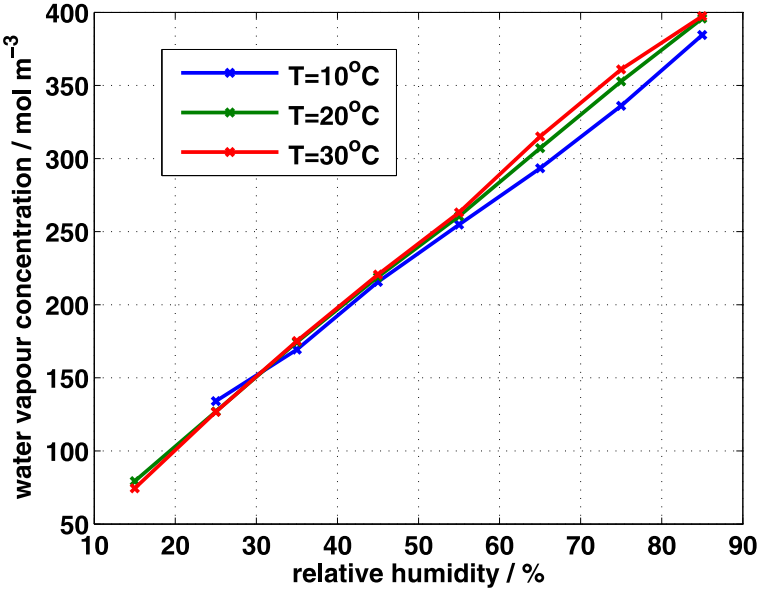

Fig. 3. Calibration of a P14 Rapid humidity sensor. Calibration was done at three different temperatures.

AMTD
7, 4407–4438, 2014

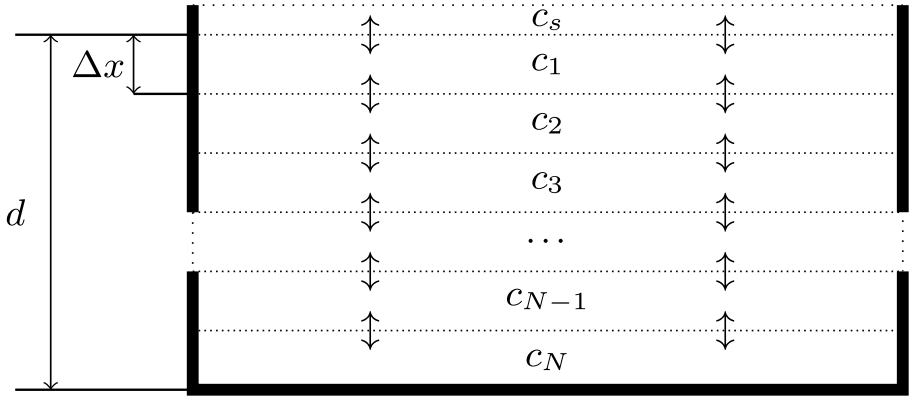

Fig. 4. Sketch of the sensor model.

AMTD
7, 4407–4438, 2014

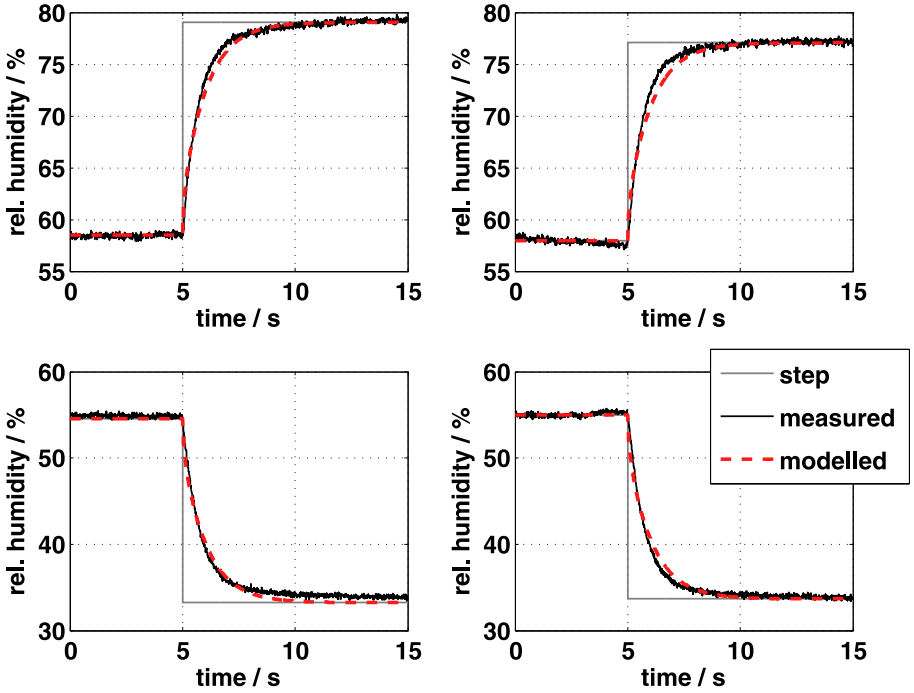

Fig. 5. Result of a step response experiment with rising edge (upper figures) and falling edge (lower figures) humidity in comparison to model results. The model was run with 40 layers and a diffusion coefficient $D = 0.38\,\mu m^2\,s^{-1}$ in all cases.

AMTD
7, 4407–4438, 2014

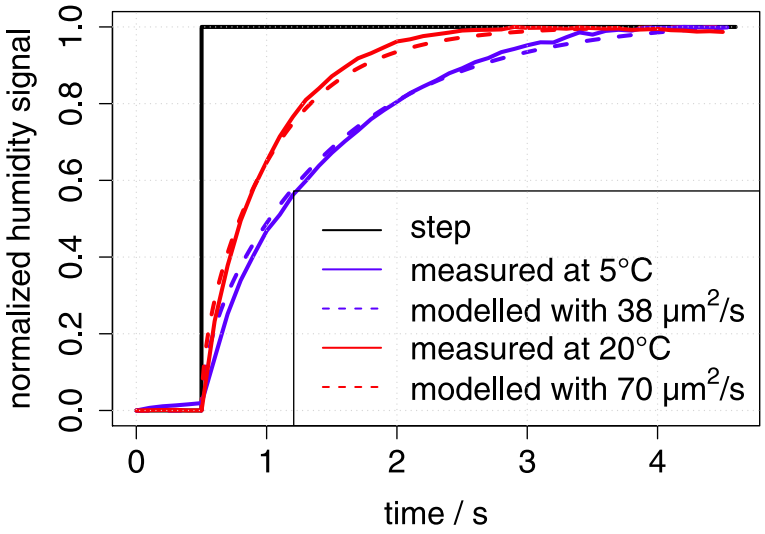

Fig. 6. Step responses of the same sensor at different temperatures. The *y* axis is normalized to zero for humidity before the step and one for humidity after the step. This is legitimate since the dynamics are not depending on the step amplitude.

AMTD
7, 4407–4438, 2014

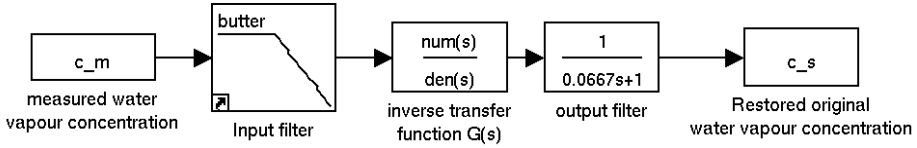

Fig. 7. Block diagram of signal restoration. The input signal of the humidity sensor is filtered with a Butterworth filter of order 20 at a cutoff frequency of 10 Hz. After the inverse transformation the signal is filtered again with a simple first order delay lowpass with cutoff frequency at 15 Hz.

AMTD
7, 4407–4438, 2014

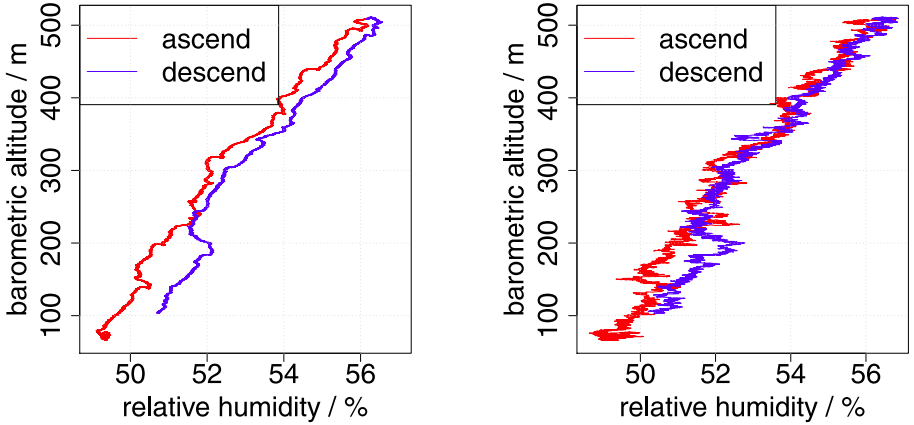

Fig. 8. Vertical profile of relative humidity before and after correction.

AMTD
7, 4407–4438, 2014

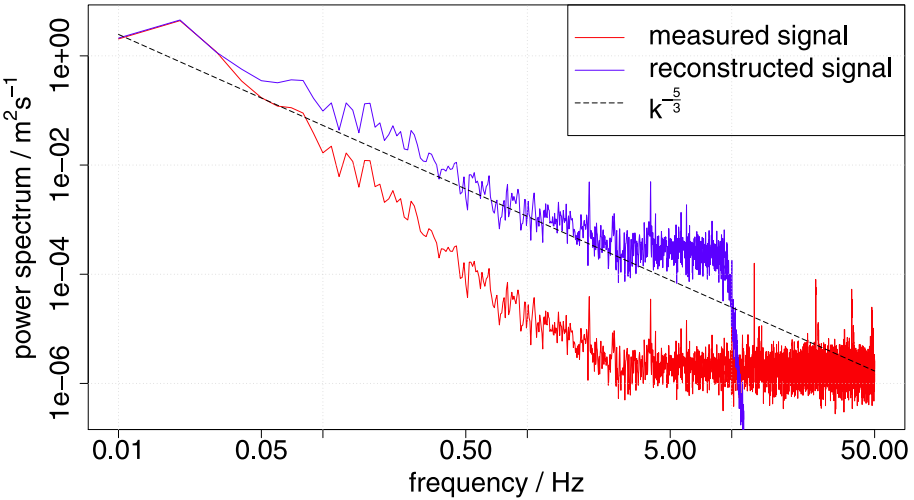

Fig. 9. Power spectrum of relative humidity before and after correction. The number of layers in the sensor model is set to $N = 40$. The diffusion constant was found to be $D = 0.1\ \mu m^2\ s^{-1}$ from the vertical profile. The spectrum is averaged over five flight legs.

AMTD
7, 4407–4438, 2014

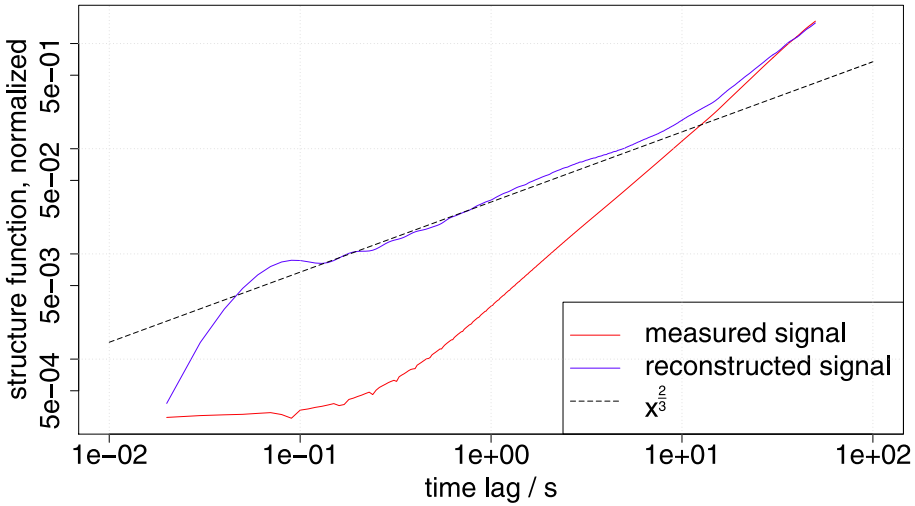

Fig. 10. Structure function before and after correction.The number of layers in the sensor model is set to $N = 40$. The diffusion constant was found to be $D = 0.1\,\mu^2\,m\,s^{-1}$ from the vertical profile. The structure function is normalized by $2\sigma^2$ and averaged over five flight legs.

AMTD
7, 4407–4438, 2014